

## Chiral valley phonons and flat phonon bands in moiré materials

Indrajit Maity , Arash A. Mostofi , and Johannes Lischner \*

*Departments of Materials and Physics and the Thomas Young Centre for Theory and Simulation of Materials, Imperial College London, South Kensington Campus, London SW7 2AZ, United Kingdom*

 (Received 13 August 2021; revised 22 December 2021; accepted 3 January 2022; published 14 January 2022)

We investigate the chirality of phonon modes in twisted bilayer  $\text{WSe}_2$  and demonstrate distinct chiral behavior of the  $K/K'$  valley phonons for twist angles close to  $0^\circ$  and close to  $60^\circ$ . In particular, multiple chiral nondegenerate  $K/K'$  valley phonons are found for twist angles near  $60^\circ$  whereas no nondegenerate chiral modes are found for twist angles close to  $0^\circ$ . Moreover, we discover two sets of emergent chiral valley modes that originate from an inversion symmetry breaking at the moiré scale and find similar modes in moiré patterns of strain-engineered bilayers  $\text{WSe}_2$  and  $\text{MoSe}_2/\text{WSe}_2$  heterostructures. At the energy gap between acoustic and optical modes, the formation of flat phonon bands for a broad range of twist angles is observed in twisted bilayer  $\text{WSe}_2$ . Our findings are relevant for understanding electron-phonon and exciton-phonon scattering in moiré materials and also for the design of phononic analogues of flat band electrons.

DOI: [10.1103/PhysRevB.105.L041408](https://doi.org/10.1103/PhysRevB.105.L041408)

**Introduction.** Chirality—the characteristic of an object that can be distinguished from its mirror image—plays a fundamental role in physics, chemistry, and biology. For example, different enantiomers of chiral molecules absorb different amounts of right-handed and left-handed polarized light, which enables their spectroscopic characterization through measurement of the circular dichroism [1]. In condensed matter physics, the chirality of electrons gives rise to many exotic effects, such as Klein tunneling [2] in graphene and the chiral magnetic effect in three-dimensional semi-metals [3,4].

Recently, the study of chirality in phonons has attracted significant interest. For example, Zhang and Niu [5] predicted the existence of chiral phonons at the  $K$  and  $K'$  valleys of monolayer  $\text{WSe}_2$ , which was subsequently verified by experiments that measured the circular dichroism of phonon-assisted intervalley transitions of holes [6]. The interaction of such chiral valley phonons with other quasiparticles is relevant for understanding and controlling many electronic and optical phenomena [7–13]. For instance, Li *et al.* demonstrated that the coupling between a chiral valley phonon and an intervalley exciton in monolayer  $\text{WSe}_2$  can lead to a long exciton lifetime maintaining the valley polarization, which is important for valley excitonics [12]. Chen *et al.* observed the entanglement of chiral phonon modes in monolayer  $\text{WSe}_2$  and single photons emitted from an embedded quantum dot in the material, which promises to reveal new avenues for phonon-driven entanglement of quantum dots [14].

Besides monolayer  $\text{WSe}_2$ , chiral phonons were found in other materials [15–19]. A particularly promising platform for observing and manipulating chiral phonons are twisted bilayers of two-dimensional (2D) materials. Since the discovery of flat, electronic bands in twisted bilayer graphene [20], such moiré materials have emerged as rich systems to investigate

the properties of correlated electrons, excitons, and phonons [21–42]. For example, at small twist angles phonon properties are significantly modified as a consequence of large atomic reconstructions [38,43,44], which result in the localization of incipient phason modes [45] and optical phonon modes [45–51]. To date, however, the chirality of phonons in twisted bilayer systems has not been studied.

In this Letter, we study the chirality of phonon modes in moiré materials. Focusing on twisted bilayer  $\text{WSe}_2$ , we first demonstrate qualitatively different phonon chiralities for twist angles close to  $0^\circ$  and close to  $60^\circ$  and explain these differences by analyzing the folding of the monolayer  $K$  and  $K'$  valleys into the Brillouin zone of the twisted bilayer. For twist angles near  $60^\circ$ , we find two sets of emergent chiral phonons modes which originate from symmetry breaking at the moiré scale. Finally, we discover flat, chiral phonon bands in the energy gap between acoustic and optical modes without the requirement of a magic angle. Such flat phonon bands were recently reported in metamaterials [52–55], but not yet in moiré systems.

**Methods.** For twist angles near  $0^\circ$  ( $\theta$ ) or  $60^\circ$  ( $60^\circ - \theta$ ), the size of the moiré unit cell becomes very large, making standard first-principles approaches for calculating phonon properties unfeasible. We therefore use simpler models for interatomic interactions. Specifically, intralayer interactions in  $\text{WSe}_2$  and  $\text{MoSe}_2$  are described using a Stillinger-Weber potential, which has been demonstrated to give accurate results for monolayers [56,57]. For interlayer interactions, we use the Kolmogorov-Crespi potential that can correctly reproduce the interlayer binding energy landscape obtained using first-principles calculations [58]. The relaxed atomic positions of our twisted bilayer systems are determined using the implementation of these potentials within the LAMMPS code [59]. Phonon frequencies and polarization vectors are obtained by diagonalizing the dynamical matrix using a modified version of the PHONOPY code [60] (see Supplementary Material (SM),

\*j.lischner@imperial.ac.uk

Sec. I, for additional details). For monolayer graphene, we use the reactive empirical bond-order (REBO) potential [61].

Following Zhang and Niu [5], we define the chirality of a phonon with crystal momentum  $\mathbf{q}$  and band index  $n$  along the  $z$ -direction (assuming that the 2D material lies in the  $x$ - $y$  plane) as

$$\begin{aligned} S_{n\mathbf{q}}^z &= \langle \epsilon_{n\mathbf{q}} | \hat{S}^z | \epsilon_{n\mathbf{q}} \rangle \\ &= \langle \epsilon_{n\mathbf{q}} | \sum_{j=1}^N [|R_j\rangle \langle R_j| - |L_j\rangle \langle L_j|] | \epsilon_{n\mathbf{q}} \rangle, \end{aligned} \quad (1)$$

where  $|\epsilon_{n\mathbf{q}}\rangle$  is the normalized polarization vector,  $\hat{S}^z$  denotes the phonon circular polarization operator, and  $N$  is the number of atoms in the moiré unit cell.  $|R_j\rangle$  and  $|L_j\rangle$  denote the right and left circularly polarized basis vectors for atom  $j$ . For example, for the first two atoms these basis vectors are given by  $|R_1\rangle = 1/\sqrt{2} \times (1, i, 0, 0, \dots)^T$ ,  $|L_1\rangle = 1/\sqrt{2} \times (1, -i, 0, 0, \dots)^T$ ,  $|R_2\rangle = 1/\sqrt{2} \times (0, 0, 1, i, 0, 0, \dots)^T$ , and  $|L_2\rangle = 1/\sqrt{2} \times (0, 0, 1, -i, 0, 0, \dots)^T$ . The phonon mode is linearly polarized when  $S_{n\mathbf{q}}^z = 0$ , circularly polarized when  $S_{n\mathbf{q}}^z = \pm 1$ , and elliptically polarized when  $0 < |S_{n\mathbf{q}}^z| < 1$ . We refer to both the circularly and elliptically polarized modes as chiral phonons. Note that for systems with time-reversal symmetry, we have  $S_{n\mathbf{q}}^z = -S_{n-\mathbf{q}}^z$ , whereas systems with inversion-symmetry obey  $S_{n\mathbf{q}}^z = S_{n-\mathbf{q}}^z$ . Therefore, the existence of *nondegenerate* chiral phonon modes requires the breaking of one of these symmetries [5,6].

As a test, we first study the chirality of phonons in monolayer graphene (which has both time-reversal and inversion symmetry) and monolayer WSe<sub>2</sub> (which is not inversion symmetric). The results are shown in Sec. II of the SM [62]. As expected, all graphene phonons are achiral. For WSe<sub>2</sub>, we find multiple *nondegenerate* chiral phonon modes near the  $K$  and  $K'$  valleys, consistent with previous first-principles calculations [6], and the signs of the chiralities in the two valleys are opposite.

*Chiral valley phonons in twisted bilayer WSe<sub>2</sub>.* The naturally occurring bilayer WSe<sub>2</sub> has 2H stacking and is inversion symmetric [64]. The untwisted bilayer, therefore, does not exhibit chiral valley phonons. However, the introduction of a twist between the layers results in the emergence of chiral phonons, as demonstrated in Figs. 1(a) and 1(b), which show the phonon chirality  $S^z$  of each phonon mode at twist angles of 21.78° and 38.22°, respectively. At 21.78°, all phonons near the  $K_M$  and  $K'_M$  valleys are achiral (with the subscript  $M$  denoting that these  $k$ -points belong to the moiré Brillouin zone), but there are some chiral phonons between  $\Gamma_M$  and  $M_M$ . In contrast, we find several chiral phonon modes in the  $K_M/K'_M$  valleys for the 38.22° twist angle (but none between  $\Gamma_M$  and  $M_M$ ). Qualitatively similar results are found for other twist angles near 0° and 60°, respectively.

The different behavior of the  $K_M/K'_M$  valley phonons for twist angles near 0° and near 60° can be understood by analyzing the folding of the monolayer phonon modes into the smaller moiré Brillouin zone (BZ). For the untwisted system (i.e.,  $\theta = 0^\circ$ ), the  $K$  point of the top layer (denoted  $K_t$ ) coincides with the  $K$  point of the bottom layer (denoted  $K_b$ ) and similarly  $K'_t$  and  $K'_b$  coincide. When instead a small, but finite twisted angle is considered, the BZs of the two layers

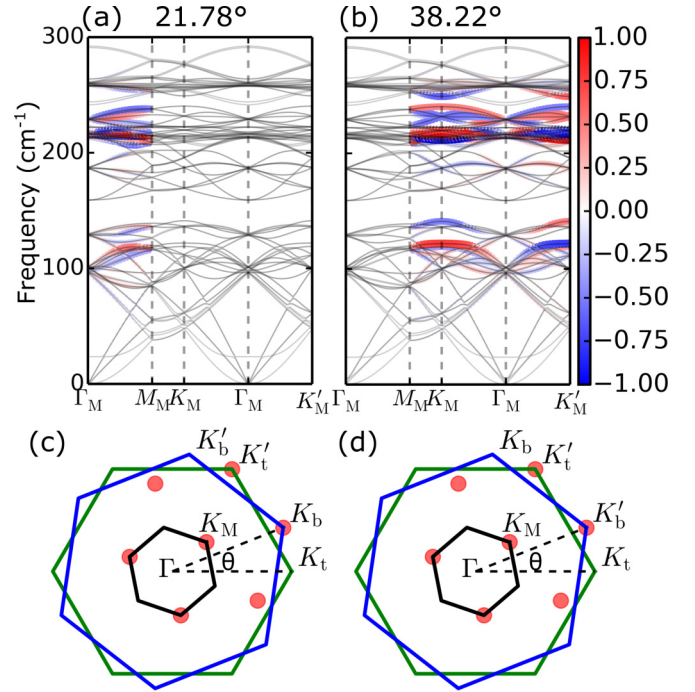


FIG. 1. [(a),(b)] Chiral phonons in twisted bilayer WSe<sub>2</sub> at twist angles of 21.78° and 38.22°, respectively. Dark solid lines represent phonon bands and the blue and red color indicates the associated chirality. [(c),(d)] Red circles denote the unfolded  $K_M$  point of the moiré BZ into the monolayer BZ for 21.78° and 38.22°, respectively. The green and blue solid lines represent the unrotated and rotated monolayer BZs, whereas the black solid line represents the moiré BZ.

are rotated relative to each other and a smaller moiré BZ is created, see Fig. 1(c). To understand which crystal momenta  $\mathbf{q}_i$  of the monolayer BZs fold onto a specific point  $\mathbf{Q}_M$  in the moiré BZ, we “unfold”  $\mathbf{Q}_M$  by adding all possible reciprocal lattice vectors  $\mathbf{G}_i$  corresponding to the moiré crystal according to [65]

$$\mathbf{q}_i = \mathbf{Q}_M + \mathbf{G}_i. \quad (2)$$

Figure 1(c) shows the set of points in the monolayer BZs that result from unfolding  $K_M$  for a twist angle of 21.78°. It can be seen that both  $K'_t$  and  $K_b$  fold onto  $K_M$ . Since the chirality of the phonons at  $K'_t$  and  $K_b$  have equal magnitudes, but opposite signs, the phonons of the twisted system have a vanishing chirality.

Instead, for the system with 60° twist angle,  $K_t$  coincides with  $K'_b$  and similarly  $K'_t$  and  $K_b$  coincide. Figure 1(d) shows that for a twist angle near 60°,  $K_M$  unfolds onto  $K'_t$  and  $K'_b$ , which have phonons with the same chirality sign. As a consequence, the phonons of the twisted bilayer exhibit a nonvanishing chirality at the  $K_M$  valley (and also for the  $K'_M$  valley).

Figure 2(a) shows the chiralities of phonons in the  $K_M$ -valley as a function of twist angle near 60° (columns labeled  $\beta$ ) and compares them to the WSe<sub>2</sub> monolayer result (the first column) and also to the results of *decoupled* twisted bilayers at the same twist angles (columns labeled  $\alpha$ ), in which no interlayer interactions between the layers are considered.

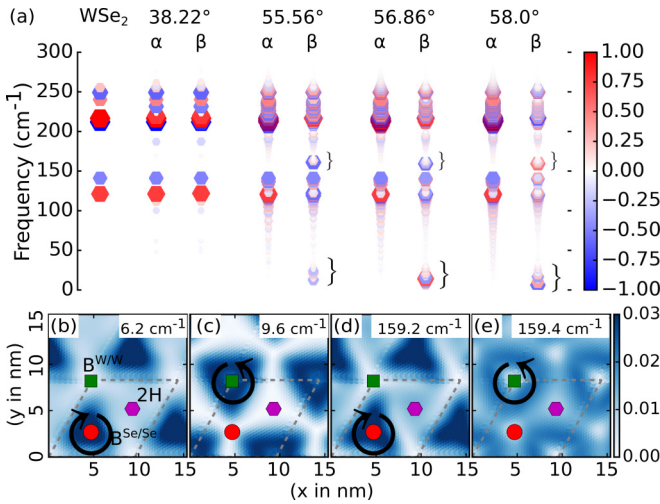


FIG. 2. (a) Chiral  $K$ -valley phonon modes of monolayer  $\text{WSe}_2$  (first column) and twisted bilayer  $\text{WSe}_2$  at different twist angles (columns labeled  $\beta$ ). For comparison, results are also shown for twisted bilayers without interlayer interactions (columns labeled  $\alpha$ ). The color of the symbols indicates the chirality of the phonon modes. The emergent chiral modes are highlighted by curly brackets. (b)–(e) Absolute value of the in-plane components of the normalized polarization vector for some of the chiral modes for a twist angle of  $58^\circ$ . In (b) and (c), the polarization vector of W atoms in the top layer is used. In (d) and (e), the polarization vector of Se atoms in the top layer is shown. Different stacking locations and associated chiralities within the moiré unit cell, which is denoted by dashed lines, are indicated.

Note that no atomic relaxations occur in decoupled twisted bilayers. For a twist angle of  $38.22^\circ$ , the phonon chiralities of the twisted bilayer are very similar to those of the monolayer and also to those of the decoupled system. As the twist angle approaches  $60^\circ$ , two novel sets of chiral valley phonons emerge [indicated by the curly brackets in Fig. 2(a)] in the twisted system which are absent in the monolayer and in the decoupled bilayer: one set with frequencies near  $10 \text{ cm}^{-1}$  and the other with frequencies near  $160 \text{ cm}^{-1}$ . The frequencies of the first set soften as the twist angle approaches  $60^\circ$ .

To understand the origin of these emergent chiral valley phonons, we plot the magnitude of the polarization vector in the moiré unit cell for  $58^\circ$ , see Figs. 2(b) to 2(e). Figures 2(b) to 2(c) show results for the two emergent valley phonons with the largest chiralities from the low-energy set (near  $10 \text{ cm}^{-1}$ ). In particular, the mode with  $6.2 \text{ cm}^{-1}$  has a chirality of  $-0.56$  and is localized in the  $B^{\text{Se/Se}}$  stacking regions while the one with  $9.6 \text{ cm}^{-1}$  has a chirality of  $0.35$  and is localized in the  $B^{\text{W/W}}$  stacking regions. Analyzing the contributions to the total chirality of these modes, we find that both layers and both W and Se atoms contribute. Figures 2(d) and 2(e) show the polarization vectors of the two valley phonons belonging to the second emergent set (with frequencies near  $160 \text{ cm}^{-1}$ ) that have the largest chiralities. The mode with frequency  $159.2 \text{ cm}^{-1}$  is localized in the  $B^{\text{Se/Se}}$  region while the one with frequency  $159.4 \text{ cm}^{-1}$  is approximately localized around the  $B^{\text{W/W}}$  region. Interestingly, only the Se atoms contribute to the total chiralities of these modes.

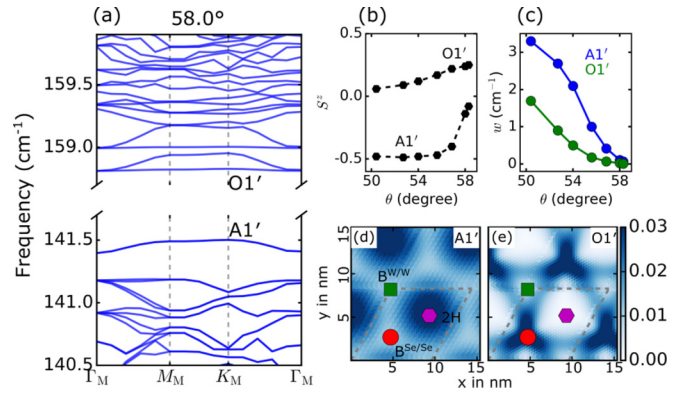


FIG. 3. (a) The phonon band structure of twisted bilayer  $\text{WSe}_2$  at  $58^\circ$  in the vicinity of the energy gap between acoustic and optical modes. (b) Chirality  $S^z$  and (c) band width of flat acoustic ( $A1'$ ) and optical ( $O1'$ ) phonon bands as function of twist angle near  $60^\circ$ . [(d),(e)] Polarization vectors of  $A1'$  and  $O1'$  modes at a twist angle of  $58^\circ$ . Different stackings are indicated by colored symbols and the moiré unit cell is outlined using dashed gray lines. In (d), the displacements of W atoms in the top layer is shown, while in (e) that of Se atoms in the top layer was used.

The emergence of these novel chiral valley phonons can be explained by an inversion symmetry breaking on the moiré scale that occurs as the twist angle approaches  $60^\circ$ . Near this twist angle, the moiré unit cell contains three high-symmetry stackings:  $2H$ ,  $B^{\text{W/W}}$ , and  $B^{\text{Se/Se}}$ . Among these stackings  $2H$  is most stable and for twist angles larger than  $\sim 55^\circ$  atomic relaxations results in a significant increase in the regions with  $2H$  stacking as well as the formation of domain walls [43] (see SM, Sec. III). It can be shown [43] that this system can be mapped onto an equivalent system of two particles (with one particle representing  $B^{\text{W/W}}$  regions and the other  $B^{\text{Se/Se}}$  regions) that occupy different sublattices of a triangular lattice and are connected by springs. Since the energies of  $B^{\text{W/W}}$  and  $B^{\text{Se/Se}}$  regions are different, the two particles have different masses and therefore the effective system lacks inversion symmetry. This, in turn, results in the emergence of novel chiral phonon modes. In contrast, the twisted bilayer near  $0^\circ$  features three high-symmetry stackings:  $AA$ ,  $B^{\text{Se/W}}$ , and  $B^{\text{W/Se}}$ . Among these stackings  $B^{\text{Se/W}}$  and  $B^{\text{W/Se}}$  are the most stable stackings. This system can be mapped onto a set of particles (representing the  $AA$  regions), which occupy the sites of a triangular lattice and are connected by springs. This effective system exhibits inversion symmetry and therefore no emergent chiral phonon modes are observed.

Our analysis shows that the polarization vectors of chiral phonons near  $0^\circ$  and  $60^\circ$  are qualitatively different from those of the monolayer phonons. This suggests that commonly used approaches for calculating phonon properties in twisted bilayers that are based on a zone-folding procedure of monolayer results are unreliable [66,67].

*Phononic band flattening in twisted bilayer  $\text{WSe}_2$ .* Figure 3(a) demonstrates the emergence of flat phonon bands in the vicinity of the energy gap between acoustic and optical modes for a  $58^\circ$  twisted bilayer. This phononic band gap is inherited from the monolayer, which has an energy gap of  $17.9 \text{ cm}^{-1}$  between the acoustic and optical phonon modes

with the highest-energy acoustic mode being located at  $K$  and the lowest-energy optical mode at the  $\Gamma$  point of the BZ. The highest-energy acoustic mode at  $K$  is nondegenerate and chiral with  $S^z = -0.5$ , while the lowest-energy optical modes at  $\Gamma$  are degenerate and achiral. Figure 3(b) shows that the chirality associated with the highest-energy acoustic mode at  $K_M$  (denoted as  $A1'$ ) changes dramatically and becomes achiral as the twist angle approaches  $60^\circ$ . This change in chirality is caused by the localization of the phonon mode in regions with inversion-symmetric  $2H$  stacking (see discussion below). In contrast, the lowest-energy optical mode at  $K_M$  (denoted as  $O1'$ ) becomes chiral as the twist angle approaches  $60^\circ$ . Figure 3(c) shows the bandwidths of the  $A1'$  and  $O1'$  modes and demonstrates that these bands become extremely flat as the twist angle approaches  $60^\circ$  and the size of the moiré cell increases. Similar to the electronic bandwidths in twisted transition-metal dichalcogenide bilayers, the flattening does not occur at a specific magic angle, unlike the case of twisted bilayer graphene [20]. Interestingly, the widths of the flat phonon bands are significantly smaller than the width of the flat electron bands at the same twist angle. For example, at a twist angle of  $56.5^\circ$  of the twisted bilayer of transition-metal dichalcogenide (TMDs), the width of the electronic valence band is 5 meV [27] and the width of the largest acoustic phonon band is 0.1 meV.

The flattening of the phonon bands is a consequence of both zone folding and the localization of phonons in real space (see SM, Sec. IV for details). Figures 3(d) and 3(e) show the polarization vectors (at  $K_M$ ) of the  $A1'$  and  $O1'$  modes for a twist angle of  $58^\circ$ . The  $A1'$  mode is localized in regions of  $2H$  stacking, while  $O1'$  is localized in  $B^{Se/Se}$  regions as well as the domain walls. It is interesting to note that the localization of the highest acoustic phonons is strikingly similar to that of the highest electronic valence states in these systems [68]. Similar band flattening is also observed for twist angles near  $0^\circ$  (see SM [62], Sec. IV), where the highest-energy acoustic mode is localized in the  $B^{W/Se}/B^{Se/W}$  stacking region and the lowest-energy optical mode is localized in regions of  $AA$  stacking and domain walls.

The distinct localization of the acoustic and optical modes can be explained by analyzing the frequencies of these modes in the various untwisted bilayers with high-symmetry stacking arrangements. For example, the  $A1'$  mode originates from the

$K$  point of the monolayer BZ. For the untwisted bilayers, the phonon frequencies at  $K$  are  $141.08 \text{ cm}^{-1}$  for  $B^{Se/Se}$  stacking,  $141.1 \text{ cm}^{-1}$  for  $B^{W/W}$  stacking and  $141.8 \text{ cm}^{-1}$  for  $2H$  stacking. Therefore, the highest-energy acoustic mode localizes on the  $2H$  regions as the moiré unit cell increases in size.

*Chiral valley phonons in strain-engineered moiré materials and heterostructures.* Besides twisting, there are two approaches to create a moiré pattern in bilayer systems: (i) by applying strain to only one of two identical layers and (ii) by stacking two different 2D materials on top of each other. We investigate the existence of chiral valley phonons in both cases. In contrast to the twisted bilayer at small twist angles, we find that the strain-engineered bilayer exhibits chiral phonons in the  $K_M$  valley (see Sec. V of the SM for a summary of these modes and more details [62]). In addition, emergent chiral phonon modes with frequencies of  $\sim 10 \text{ cm}^{-1}$  and  $\sim 156 \text{ cm}^{-1}$  are found. Finally, we also observe emergent chiral phonon modes in a  $WSe_2/MoSe_2$  heterostructure at a twist angle of  $3.14^\circ$  (see SM [62], Sec. V).

*Summary.* In this Letter, we demonstrated the presence of chiral phonons in twisted bilayer  $WSe_2$  as well as other moiré materials and studied their properties. We found that the phonon chirality depends on the twist angle with systems near  $0^\circ$  exhibiting qualitatively different chiralities than systems near  $60^\circ$ . Very close to  $60^\circ$ , we observe emergent chiral modes as well as flat phonon bands. The predicted chiral properties of phonons in twisted bilayer materials can be measured with helicity-resolved Raman spectroscopy [15,69]. While the resolution of such techniques is typically not high enough to access individual modes in systems near  $0^\circ$  and  $60^\circ$ , they can potentially measure the  $k$ -point and helicity-resolved phonon density of states (see SM, Sec. VII). Future work should investigate the scattering of chiral phonons with other quasiparticles, such as electrons, excitons, and photons and the effects of such scattering processes on the electronic and optical properties of moiré materials.

*Acknowledgments.* This project received funding from the European Union's Horizon 2020 research and innovation program under the Marie Skłodowska-Curie Grant agreement No. 101028468. The authors acknowledge support from the Thomas Young Centre under Grant No. TYC-101, and discussions with Rup Chowdhury, Nikita Tepliakov, and Saurabh Srivastav.

- 
- [1] L. M. Kneer, E.-M. Roller, L. V. Besteiro, R. Schreiber, A. O. Govorov, and T. Liedl, *ACS Nano* **12**, 9110 (2018).
- [2] M. I. Katsnelson, K. S. Novoselov, and A. K. Geim, *Nat. Phys.* **2**, 620 (2006).
- [3] Q. Li and D. E. Kharzeev, *Nucl. Phys. A* **956**, 107 (2016), the XXV International Conference on Ultrarelativistic Nucleus-Nucleus Collisions: Quark Matter 2015.
- [4] Q. Li, D. E. Kharzeev, C. Zhang, Y. Huang, I. Pletikosiá, A. V. Fedorov, R. D. Zhong, J. A. Schneeloch, G. D. Gu, and T. Valla, *Nat. Phys.* **12**, 550 (2016).
- [5] L. Zhang and Q. Niu, *Phys. Rev. Lett.* **115**, 115502 (2015).
- [6] H. Zhu, J. Yi, M.-Y. Li, J. Xiao, L. Zhang, C.-W. Yang, R. A. Kaindl, L.-J. Li, Y. Wang, and X. Zhang, *Science* **359**, 579 (2018).
- [7] B. R. Carvalho, Y. Wang, S. Mignuzzi, D. Roy, M. Terrones, C. Fantini, V. H. Crespi, L. M. Malard, and M. A. Pimenta, *Nat. Commun.* **8**, 14670 (2017).
- [8] S.-Y. Chen, C. Zheng, M. S. Fuhrer, and J. Yan, *Nano Lett.* **15**, 2526 (2015).
- [9] M. Kang, S. W. Jung, W. J. Shin, Y. Sohn, S. H. Ryu, T. K. Kim, M. Hoesch, and K. S. Kim, *Nat. Mater.* **17**, 676 (2018).
- [10] Z. Li, T. Wang, C. Jin, Z. Lu, Z. Lian, Y. Meng, M. Blei, S. Gao, T. Taniguchi, K. Watanabe, T. Ren, S. Tongay, L. Yang, D. Smirnov, T. Cao, and S.-F. Shi, *Nat. Commun.* **10**, 2469 (2019).

- [11] E. Liu, J. van Baren, T. Taniguchi, K. Watanabe, Y.-C. Chang, and C. H. Lui, *Phys. Rev. Research* **1**, 032007(R) (2019).
- [12] Z. Li, T. Wang, C. Jin, Z. Lu, Z. Lian, Y. Meng, M. Blei, M. Gao, T. Taniguchi, K. Watanabe, T. Ren, T. Cao, S. Tongay, D. Smirnov, L. Zhang, and S.-F. Shi, *ACS Nano* **13**, 14107 (2019).
- [13] A. Delhomme, D. Vaclavkova, A. Slobodeniuk, M. Orlita, M. Potemski, D. M. Basko, K. Watanabe, T. Taniguchi, D. Mauro, C. Barreateau, E. Giannini, A. F. Morpurgo, N. Ubrig, and C. Faugeras, *2D Mater.* **7**, 041002 (2020).
- [14] X. Chen, X. Lu, S. Dubey, Q. Yao, S. Liu, X. Wang, Q. Xiong, L. Zhang, and A. Srivastava, *Nat. Phys.* **15**, 221 (2019).
- [15] H. Chen, W. Zhang, Q. Niu, and L. Zhang, *2D Mater.* **6**, 012002 (2018).
- [16] D. M. Juraschek and N. A. Spaldin, *Phys. Rev. Materials* **3**, 064405 (2019).
- [17] L. Du, J. Tang, Y. Zhao, X. Li, R. Yang, X. Hu, X. Bai, X. Wang, K. Watanabe, T. Taniguchi, D. Shi, G. Yu, X. Bai, T. Hasan, G. Zhang, and Z. Sun, *Adv. Funct. Mater.* **29**, 1904734 (2019).
- [18] W. Zhang, A. Srivastava, X. Li, and L. Zhang, *Phys. Rev. B* **102**, 174301 (2020).
- [19] G. Grissonnanche, S. Thériault, A.ourgout, M.-E. Boulanger, E. Lefrancois, A. Ataei, F. Laliberté, M. Dion, J.-S. Zhou, S. Pyon, T. Takayama, H. Takagi, N. Doiron-Leyraud, and L. Taillefer, *Nat. Phys.* **16**, 1108 (2020).
- [20] R. Bistritzer and A. H. MacDonald, *Proc. Natl. Acad. Sci. USA* **108**, 12233 (2011).
- [21] Y. Cao, V. Fatemi, S. Fang, K. Watanabe, T. Taniguchi, E. Kaxiras, and P. Jarillo-Herrero, *Nature (London)* **556**, 43 (2018).
- [22] Y. Cao, V. Fatemi, A. Demir, S. Fang, S. L. Tomarken, J. Y. Luo, J. D. Sanchez-Yamagishi, K. Watanabe, T. Taniguchi, E. Kaxiras, R. C. Ashoori, and P. Jarillo-Herrero, *Nature (London)* **556**, 80 (2018).
- [23] K. Tran, J. Choi, and A. Singh, *2D Mater.* **8**, 022002 (2020).
- [24] L. Wang, E.-M. Shih, A. Ghiotto, L. Xian, D. A. Rhodes, C. Tan, M. Claassen, D. M. Kennes, Y. Bai, B. Kim, K. Watanabe, T. Taniguchi, X. Zhu, J. Hone, A. Rubio, A. N. Pasupathy, and C. R. Dean, *Nat. Mater.* **19**, 861 (2020).
- [25] M. Huang, Z. Wu, J. Hu, X. Cai, E. Li, L. An, X. Feng, Z. Ye, N. Lin, K. T. Law *et al.*, [arXiv:2006.05615](https://arxiv.org/abs/2006.05615).
- [26] G. Scuri, T. I. Andersen, Y. Zhou, D. S. Wild, J. Sung, R. J. Gelly, D. Bérubé, H. Heo, L. Shao, A. Y. Joe, A. M. Mier Valdivia, T. Taniguchi, K. Watanabe, M. Lončar, P. Kim, M. D. Lukin, and H. Park, *Phys. Rev. Lett.* **124**, 217403 (2020).
- [27] M. H. Naik and M. Jain, *Phys. Rev. Lett.* **121**, 266401 (2018).
- [28] Z. Zhang, Y. Wang, K. Watanabe, T. Taniguchi, K. Ueno, E. Tutuc, and B. J. LeRoy, *Nat. Phys.* **16**, 1093 (2020).
- [29] L. An, X. Cai, D. Pei, M. Huang, Z. Wu, Z. Zhou, J. Lin, Z. Ying, Z. Ye, X. Feng, R. Gao, C. Cacho, M. Watson, Y. Chen, and N. Wang, *Nanoscale Horiz.* **5**, 1309 (2020).
- [30] L. Xian, M. Claassen, D. Kiese, M. M. Scherer, S. Trebst, D. M. Kennes, and A. Rubio, *Nat. Commun.* **12**, 5644 (2021).
- [31] T. Devakul, V. Crépel, Y. Zhang, and L. Fu, *Nat. Commun.* **12**, 6730 (2021).
- [32] V. Vitale, K. Atalar, A. A. Mostofi, and J. Lischner, [arXiv:2102.03259](https://arxiv.org/abs/2102.03259).
- [33] S. Venkateswarlu, A. Honecker, and G. Trambly de Laissardière, *Phys. Rev. B* **102**, 081103(R) (2020).
- [34] E. Li, J.-X. Hu, X. Feng, Z. Zhou, L. An, K. T. Law, N. Wang, and N. Lin, *Nat. Commun.* **12**, 5601 (2021).
- [35] D. Soriano and J. Lado, *New J. Phys.* **23**, 073038 (2021).
- [36] S. Shabani, D. Halbertal, W. Wu, M. Chen, S. Liu, J. Hone, W. Yao, D. N. Basov, X. Zhu, and A. N. Pasupathy, *Nat. Phys.* **17**, 720 (2021).
- [37] S. Brem, K.-Q. Lin, R. Gillen, J. M. Bauer, J. Maultzsch, J. M. Lupton, and E. Malic, *Nanoscale* **12**, 11088 (2020).
- [38] A. Weston, Y. Zou, V. Enaldiev, A. Summerfield, N. Clark, V. Zólyomi, A. Graham, C. Yelgel, S. Magorrian, M. Zhou, J. Zultak, D. Hopkinson, A. Barinov, T. H. Bointon, A. Kretinin, N. R. Wilson, P. H. Beton, V. I. Fal'ko, S. J. Haigh, and R. Gorbachev, *Nat. Nanotechnol.* **15**, 592 (2020).
- [39] S. Sinha, P. C. Adak, R. S. Surya Kanthi, B. L. Chittari, L. D. V. Sangani, K. Watanabe, T. Taniguchi, J. Jung, and M. M. Deshmukh, *Nat. Commun.* **11**, 5548 (2020).
- [40] Z. A. Goodwin, L. Klebl, V. Vitale, X. Liang, V. Gogtay, X. van Gorp, D. M. Kennes, A. A. Mostofi, and J. Lischner, *Phys. Rev. Materials* **5**, 084008 (2021).
- [41] A. J. Graham, J. Zultak, M. J. Hamer, V. Zolyomi, S. Magorrian, A. Barinov, V. Kandyba, A. Giampietri, A. Locatelli, F. Genuzio, N. C. Teutsch, C. Salazar, N. D. M. Hine, V. I. Fal'ko, R. V. Gorbachev, and N. R. Wilson, *2D Mater.* **8**, 015016 (2020).
- [42] J. M. Pizarro, M. J. Calderón, and E. Bascones, *J. Phys. Commun.* **3**, 035024 (2019).
- [43] I. Maity, P. K. Maiti, H. R. Krishnamurthy, and M. Jain, *Phys. Rev. B* **103**, L121102 (2021).
- [44] S. Carr, D. Massatt, S. B. Torrisi, P. Cazeaux, M. Luskin, and E. Kaxiras, *Phys. Rev. B* **98**, 224102 (2018).
- [45] I. Maity, M. H. Naik, P. K. Maiti, H. R. Krishnamurthy, and M. Jain, *Phys. Rev. Research* **2**, 013335 (2020).
- [46] A. C. Gadelha, D. A. A. Ohlberg, C. Rabelo, E. G. S. Neto, T. L. Vasconcelos, J. L. Campos, J. S. Lemos, V. Ornelas, D. Miranda, R. Nadas, F. C. Santana, K. Watanabe, T. Taniguchi, B. van Troeye, M. Lamparski, V. Meunier, V.-H. Nguyen, D. Paszko, J.-C. Charlier, L. C. Campos *et al.*, and *Nature (London)* **590**, 405 (2021).
- [47] M. Koshino and Y.-W. Son, *Phys. Rev. B* **100**, 075416 (2019).
- [48] J. Quan, L. Linhart, M.-L. Lin, D. Lee, J. Zhu, C.-Y. Wang, W.-T. Hsu, J. Choi, J. Embley, C. Young, T. Taniguchi, K. Watanabe, C.-K. Shih, K. Lai, A. H. MacDonald, P.-H. Tan, F. Libisch, and X. Li, *Nat. Mater.* **20**, 1100 (2021).
- [49] M. Lamparski, B. V. Troeye, and V. Meunier, *2D Mater.* **7**, 025050 (2020).
- [50] K.-Q. Lin, J. Holler, J. M. Bauer, P. Parzefall, M. Scheuck, B. Peng, T. Korn, S. Bange, J. M. Lupton, and C. Schüller, *Adv. Mater.* **33**, 2008333 (2021).
- [51] R. Debnath, I. Maity, R. Biswas, V. Raghunathan, M. Jain, and A. Ghosh, *Nanoscale* **12**, 17272 (2020).
- [52] Y. Deng, M. Oudich, N. J.R.K. Gerard, J. Ji, M. Lu, and Y. Jing, *Phys. Rev. B* **102**, 180304(R) (2020).
- [53] M. Rosendo López, F. Peñaranda, J. Christensen, and P. San-Jose, *Phys. Rev. Lett.* **125**, 214301 (2020).
- [54] S. M. Gardezi, H. Pirie, S. Carr, W. Dorrell, and J. E. Hoffman, *2D Mater.* **8**, 031002 (2021).
- [55] M. Martí-Sabaté and D. Torrent, *Phys. Rev. Appl.* **15**, L011001 (2021).
- [56] A. Mobaraki, A. Kandemir, H. Yapicioglu, O. Glseren, and C. Sevik, *Comput. Mater. Sci.* **144**, 92 (2018).
- [57] A. Kandemir, H. Yapicioglu, A. Kinaci, T. Çağın, and C. Sevik, *Nanotechnology* **27**, 055703 (2016).

- [58] M. H. Naik, I. Maity, P. K. Maiti, and M. Jain, *J. Phys. Chem. C* **123**, 9770 (2019).
- [59] S. Plimpton, *J. Comput. Phys.* **117**, 1 (1995).
- [60] A. Togo and I. Tanaka, *Scr. Mater.* **108**, 1 (2015).
- [61] D. W. Brenner, O. A. Shenderova, J. A. Harrison, S. J. Stuart, B. Ni, and S. B. Sinnott, *J. Phys.: Condens. Matter* **14**, 783 (2002).
- [62] See Supplementary Material (SM) at <http://link.aps.org/supplemental/10.1103/PhysRevB.105.L041408> for simulation details, chiral phonon in monolayer graphene, WSe<sub>2</sub> and polarization vectors, interlayer separation for twist angles close to 0° and close to 60°, flat phonon bands for twist angles close to 0°, chiral valley phonons in strain-engineered moiré and MoSe<sub>2</sub>/WSe<sub>2</sub> heterostructure, and movies to illustrate distinct chiral valley phonons twist angles close to 0° and close to 60°, which includes Ref. [63].
- [63] J. M. B. Lopes dos Santos, N. M. R. Peres, and A. H. Castro Neto, *Phys. Rev. Lett.* **99**, 256802 (2007).
- [64] A. M. Jones, H. Yu, J. S. Ross, P. Klement, N. J. Ghimire, J. Yan, D. G. Mandrus, W. Yao, and X. Xu, *Nat. Phys.* **10**, 130 (2014).
- [65] V. Popescu and A. Zunger, *Phys. Rev. B* **85**, 085201 (2012).
- [66] M.-L. Lin, Q.-H. Tan, J.-B. Wu, X.-S. Chen, J.-H. Wang, Y.-H. Pan, X. Zhang, X. Cong, J. Zhang, W. Ji, P.-A. Hu, K.-H. Liu, and P.-H. Tan, *ACS Nano* **12**, 8770 (2018).
- [67] P. Parzefall, J. Holler, M. Scheuck, A. Beer, K.-Q. Lin, B. Peng, B. Monserrat, P. Nagler, M. Kempf, T. Korn, and C. Schller, *2D Mater.* **8**, 035030 (2021).
- [68] S. Kundu, M. H. Naik, H. Krishnamurthy, and M. Jain, [arXiv:2103.07447](https://arxiv.org/abs/2103.07447).
- [69] Y. Tatsumi, T. Kaneko, and R. Saito, *Phys. Rev. B* **97**, 195444 (2018).